HHS Public Access

Author manuscript

Oral Oncol. Author manuscript; available in PMC 2016 February 01.

Published in final edited form as:

Oral Oncol. 2015 February ; 51(2): 195–201. doi:10.1016/j.oraloncology.2014.11.001.

Characteristics and kinetics of cervical lymph node regression after radiation therapy for human papillomavirus-associated oropharyngeal carcinoma: Quantitative image analysis of post-radiotherapy response

Chad Tang, MD[*], **Clifton D. Fuller, MD, PhD**[*], **Adam S. Garden, MD**[*], **Musaddiq J. Awan, MD**[*], **Rivka R. Colen, MD**[‡], **William H. Morrison, MD**[*], **Steven J. Frank, MD**[*], **Beth M. Beadle, MD, PhD**[*], **Jack Phan, MD, PhD**[*], **Erich M. Sturgis, MD, MPH**[**], **Mark E. Zafereo, MD**[**], **Randal S. Weber, MD**[**], **David I. Rosenthal, MD**[*], and **G. Brandon Gunn, MD**[*]

[*]Department of Radiation Oncology, The University of Texas MD Anderson Cancer Center, Houston, Texas, USA

[‡]Department of Diagnostic Radiology, The University of Texas MD Anderson Cancer Center, Houston, Texas, USA

[**]Department of Head and Neck Surgery, The University of Texas MD Anderson Cancer Center, Houston, Texas, USA

Abstract

Background and Purpose—We sought to characterize the pattern of lymph node regression and morphology following definitive radiation therapy (RT) for human papilloma virus (HPV)-associated oropharyngeal carcinoma in patients with disease control.

Materials and Methods—Radiographically positive cervical lymph nodes from patients treated with definitive RT for HPV-associated oropharyngeal carcinoma were segmented on initial pre- and subsequent post-RT contrast enhanced CT images. Pre-specified quantitative nodal parameters were calculated. Initial nodal parameter correlates of final nodal size, final nodal volume, and time to <1 cm short-axis diameter were determined.

Results—Sixty-six radiographically positive lymph node were analyzed in 36 patients. Lymph nodes exhibited initial volume decreases with size stabilization at ~4 months. Fifteen nodes (23%) underwent complete radiographic response (median 6.4 months following RT; range 2.9–25.6 months). On multivariate time-to-event analysis, initial hypodense/fat component, nodal volume, and short-axis diameter exhibited inverse association, while higher HU standard deviation exhibited a positive association, with reaching <1 cm short-axis diameter (all $p<0.05$).

Conclusions—Our results showed a substantial decrease in nodal volume within the first 1–2 months following RT. These findings support our current nodal imaging paradigm, propose a

Correspondence to: G. Brandon Gunn, MD, Department of Radiation Oncology, Unit 97, The University of Texas MD Anderson Cancer Center, 1515 Holcombe Blvd, Houston, TX 77030, USA. Tel: +1-713-563-2300; Fax: +1-713-404-4124; gbgunn@mdanderson.org.

Conflicts of Interest: None

quantitative methodology, and describe a reference dataset for further validation and comparison studies.

Keywords

Oropharynx cancer; HPV; radiographic response; cervical lymph nodes; quantitative methodology

Introduction

The incidence of oropharyngeal carcinoma in the United States is increasing, primarily due to human papillomavirus (HPV)-associated cases [1]. HPV-associated oropharyngeal carcinomas commonly presents with advanced regional lymph node (LN) involvement with heterogeneous nodal imaging characteristics [2]. Such nodes exhibit diverse morphologic components including solid, cystic, and necrotic elements [3, 4]. Standard treatment paradigms for oropharyngeal carcinoma have centered on definitive radiation therapy (RT), often in sequence and/or in combination with systemic therapy. Surgery, specifically neck dissection, is typically reserved for evidence of residual nodal disease on follow up imaging [5].

Contrast enhanced computed tomography (CT) of the neck (CECTN) has been the primary imaging modality for initial cervical LN staging evaluation and subsequent treatment response assessment at our institution. Whole body FDG-PET/CT, MRI neck, US neck and US-guided FNA are also integrated in select cases [6, 7]. Our current post-RT neck management paradigm includes consideration for neck dissections 8–12 weeks after RT completion and relies greatly on post-treatment CECTN imaging assessment [8–12].

We hypothesize that pretreatment cervical LN imaging characteristics influence the kinetics and pattern of radiographic LN regression and potentially impact the CECTN characteristics of the final nodal remnant. We undertook this study in order to establish a workflow to evaluate multi-parametric CT nodal regression characteristics and to create a reference dataset of radiographic LN regression patterns in a modern cohort of HPV-associated oropharyngeal carcinoma patients, with disease control following RT or concurrent chemoradiation alone (i.e. without neck dissection). The specific aims of the current study included: 1) quantitative characterization of radiographic nodal regression in HPV-associated oropharyngeal carcinoma radiation responders over time; 2) identification of quantitative imaging parameters as correlates of nodal regression; 3) generation of testable hypotheses for future comparison and prospective research.

Material and Methods

Patients

Following Institutional Review Board approval, departmental databases were searched to identify adult patients irradiated at our institution for LN-positive HPV-associated oropharyngeal carcinoma. HPV status was determined by review of the medical records and pathology reports. Cases were considered HPV-associated if tested tumor specimens were positive for p16 by immunohistochemistry or high-risk HPV DNA by in-situ hybridization.

Inclusion criteria were: 1) treatment with definitive RT with or without concurrent systemic therapy; 2) pre-treatment CECTN DICOM images available for evaluation; 3) clinical disease control with minimum of two years follow up post-RT; 4) at least two post-treatment diagnostic CECTN DICOM images over a minimum of 6 months follow up. Exclusion criteria were: 1) receipt of neoadjuvant/induction or adjuvant systemic therapy; 2) receipt of pre- or post-RT neck dissection (pre-treatment excisional LN biopsies were allowed, given that at least one radiographically evident positive LN remained for evaluation); 3) development of local, regional, or distant recurrence following initial treatments; 4) prior RT to the head or neck; 5) distant metastatic or recurrent disease at presentation.

Imaging

Pre- and post-treatment CECTN DICOM images for all cases were transferred to the Pinnacle RT treatment planning system (ver. 9.4, Phillips, Andover MA). For this study, LNs analyzed were those reported as positive on diagnostic imaging reports, identifiable on the pre-treatment diagnostic CECTN, and generally met any of the following criteria: 1) size >1.0 cm on short axis (while considering nodal level), 2) peripheral or irregular contrast enhancement, 3) presence of focal or central lucency or necrosis, 4) round rather than kidney/reniform shape, and 5) presence of radiographic extracapsular extension [10, 13–16]. As per standard RT target delineation practice, individual positive cervical LNs were manually segmented/contoured, on a slice-by-slice basis and assigned a unique region of interest (ROI).

LNs included in this study were those described and annotated as positive in initial diagnostic radiology reports. Delineation of these nodes were corroborated in a peer fashion review at our departmental bi-weekly Head and Neck Development and Planning Clinic, as previously described [17]. Post-RT nodal volumes were delineated likewise (C.T.) with 15% of cases subjected to additional peer-review (G.B.G.).

Per institutional practice, the first post-RT follow-up CECTN was typically obtained 8 weeks following RT completion, then 3–4 months thereafter during the first two years of follow up, then every 6 months up to 5 years, and subsequently on an annual basis. Imaging follow-up at our institution generally consists of CECTN with PET and MRI reserved for equivocal findings and physician preference. CECTN images were typically obtained at our institution with 1.25-mm-section thickness and 25-cm FOV. Standard imaging generally used 120-mL iohexol (Omnipaque; GE healthcare, Princeton NJ) contrast, with imaging on a multi-slice scanner (Optima, GE Healthcare, Milwaukee WI). All follow up CECTNs and 33 of 36 (92%) baseline images were conducted at our institution.

CT parameters

Quantitative CT-based nodal characteristics were determined for segmented LNs ROI at each time-point using Pinnacle treatment planning system. Associated statistics were calculated using Matlab ver. 8.0 (MathWorks, Natick MA). Preselected nodal parameters included median and mean Hounsfield units (HU), HU standard deviation, and total nodal volume. CT intensity-volume histograms (i.e. plotting HU vs. ROI volume) were generated for each LN ROI. ROI volumes were segmented into four categories by HU: <0, 0–30, 30–

170, and >170 HU. The proportion of the nodal ROI within these HU ranges were then labeled as follows: 0–30, fluid; 30–170 HU, soft tissue; <0 HU, hypodensity/fat; >170 HU, enhancement/calcification [4, 18].

For all LNs, the involved anatomic nodal station was recorded based on consensus guidelines [19] and the greatest short axis dimension in the axial plane was measured. Nodes were scored as complete radiographic responders in the event that a treated nodal remnant could not be identified visually. In such instances all nodal parameters were set to zero.

Statistical analysis

Continuous and categorical variables were compared using Fisher's exact and Wilcoxon rank-sum tests, respectively. Univariate and multivariate linear regressions were utilized to associate initial CETCN parameters with final node short-axis diameter and final volume. Final short-axis diameter and nodal volume were considered the volumes on the final reviewed post-treatment scan.

To discretize continuous variables, optimal cutpoints were calculated utilizing X-Tile software [20]. As such an analysis assesses multiple cutpoints, Miller-Seigmund *P*-values to correct for multiple comparisons are reported in addition to log-rank p-values for univariate analyses. Univariate and multivariate time-to-event analyses were conducted via Kaplan-Meier and Cox regression for the *a priori* endpoint of LN regression to <1 cm short-axis diameter. This endpoint was chosen as a conservative benchmark frequently used in our institution. Tests were two-sided when appropriate with significance considered at $p<0.05$. Statistical analyses were conducted using JMP v10 and SAS v9.3 (both SAS Institute Inc., Cary, NC).

Results

Patient and initial nodal characteristics

Between March 2004 to December 2011, 202 patients with oropharynx cancer with known HPV status were screened. Patients were excluded due to receipt of induction chemotherapy (n=125), occurrence of locoregional failure, distant metastatic failure, or death (n=11), N0 disease or excisional biopsy removing the only pathologic node (n=20), and lack of pre-treatment CECTN, inadequate followup, imaging with modalties outside of CECTN (n=10).

Within the remaining 36 patients, sixty-six radiographically positive LN ROIs were segmented and analyzed. Patient, disease, and initial nodal characteristics are shown in Table 1. The majority of patients presented with T2 (42%) and N2b (67%) with a median of 2 involved LNs (range 1–4). Nodes meeting pathologic criteria were generally included within a high dose RT target volume and treated to a median dose of 68.5 Gy (range 59.2–72.8 Gy). Representative nodes are shown in Figure 1.

Post-radiation therapy imaging and nodal regression over time

The median number of post-treatment scans reviewed per patient was 6 (range: 3–9). Median time from RT completion to the first post-treatment imaging was 1.8 months (range 1.1–5.6 months). Subsequent scans were obtained as follows: 2nd scan: median 6.2 months

(range 2.5–22 months) and 3rd scan: median 11.2 months (range 4.8–26.6 months). Nodal ROI volumes were found to exhibit a relatively large initial volume decrement at the first post-therapy CECTN, with incrementally smaller volume reduction on subsequent imaging until arriving at a nadir. Nodal ROI volume as a function of time from therapy was plotted in Figure 2a.

Initial nodal ROI volume (median 2311 mm^3, range 60–29565 mm^3) was markedly larger than at 1–2 months after RT completion (n=39, median 619 mm^3, range 106–7319 mm^3, $p<0.0001$). The median size decrease within this time interval was 80.2% (range 15.2%–97.2%). Nodal ROI volume at 1–2 months, in contrast, was not significantly greater than at 2–3 months post-therapy (n=20, median 411 mm^3, range 0–1798 mm^3, $p= 0.10$) but was significantly larger than at 3–5 months post-therapy (n=16, median 348 mm^3, range 0–1785 mm^3, $p=0.04$). ROI volumes were not distinct between 2–3 and 3–5 months in interval imaging ($p=0.45$). Fifteen nodes (23%) underwent a complete radiographic response, occurring at a median 6.4 months following RT (range 2.9–25.6 months).

Nodal imaging parameters over time

CECTN sub-volume parameters are shown with respect to time in Figure 2b. Generally, median nodal HU decreased while HU standard deviation increased following RT. In regards to HU-categorized ROI sub-volumes, soft tissue components decreased over time, while proportions of hypodense/fat and fluid increased. Eleven nodes (17%) developed a calcified component that occupied ≥5% of total volume (median 5.6 months following RT; range 1.4–23.7 months).

Final nodal size and volume

Following initial post-RT volume reduction, the rate of decrement slowed, approaching a final nadir (Fig. 2a). Median final short axis diameter for all nodal ROIs was 0.3 cm (range 0.1–0.6 cm). Nodal ROIs were measured to be within 0.1 cm of nadir short-axis diameter at a median of 12.8 months post-RT (range 2.3–26.6 months). Median final ROI volume was 98 mm^3 (range 0–771 mm^3). Nodal ROIs were determined to be within 10% of nadir volume at a median of 16.9 months post-RTRT (range 2.3–36.2 months). Resultant univariate and multivariate analyses of initial quantitative CT parameter correlates of final nodal ROI volume and final short-axis diameter are shown in Table 2. In univariate analysis, pre-therapy CT parameters associated with longer final short axis diameter were initial ROI volume and short-axis diameter (both $p<0.05$). On multivariate analysis, greater initial hypodense/fat component, median HU, and volume were associated with longer final short axis diameter (all $p<0.05$) (Table 2). Similar to final short-axis diameter, on univariate regression initial nodal parameters associated with larger final volumes were greater initial volume and short-axis diameter (both $p<0.01$). Multivariate linear regression revealed greater initial median HU and ROI volume to be associated with larger final volume (both $p<0.01$) (Table 2).

Time-to-event analysis

Forty-two LNs with initial short-axis diameters >1 cm were included in the time-to-event analysis. Optimal parameter cutpoints as calculated by X-Tiles are listed in Table 3 and

utilized for all subsequent analyses. All LNs reached a nadir short-axis diameter of <1 cm, with median time to <1 cm diameter of 2.1 months post-RT (range 1.1–22.1 months). Univariate analysis revealed initial hypodensity (HR=0.2, p=0.0008), ROI volume (HR=0.4, p=0.002), and short-axis diameter (HR=0.1, p<0.0001) to be inversely associated with regression to a short axis diameter of <1 cm. Initial ROI median HU was associated with probability of achieving <1 cm short-axis diameter (HR=2.1, p=0.02). However, adjustment for multiple comparison(s) revealed only initial ROI hypodensity and short-axis diameters pre-therapy to be significantly associated with likelihood reaching <1 cm short-axis diameter (both adjusted p<0.05). On multivariate analysis, initial pre-therapy ROI hypodense/fat sub-volume component, nodal ROI volume, and ROI short-axis diameter were found to be inversely associated with reaching <1 cm short-axis diameter (all p<0.05), while HU standard deviation was associated with reaching <0.1 short-axis diameter (HR=1.9, p=0.049) (Table 3). Representative cumulative incidence curves showing time-to <0.1 short-axis diameter stratified by initial hypodense/fat component, HU standard deviation, and nodal volumes are shown in Figure 3.

Discussion

This descriptive CT-based imaging study details the post-RT pattern and kinetics of nodal morphology in a cohort of HPV-associated oropharyngeal carcinomas exhibiting disease control. Our results showed a substantial decrease in post-treatment nodal volume across the early post-treatment period, with significant higher rates of decrease at 1–2 months versus 3–5 months post-RT. This is best illustrated in Figure 2a in which a steep initial size decrement is followed by leveling off at a nadir (Fig. 2a). This response profile highlights the potential implications of first post-treatment imaging timing, supporting our current preference to first image ≥2 months following RT, a time period in which responding treated LNs would be expected to have achieved the largest proportion of volume regression, while still allowing for timely additional imaging/biopsy or surgical intervention for non-responders. It is important to note that although the initial median decrease in volume was substantial (80.2%), some nodes exhibiting as low as 15.2% decrease. As such, further refinement of neck control criteria would optimally include factors other than size. One conservative estimate for volume threshold for consideration of a pathologically controlled node would be >50% decrease at 1–2 month post-treatment, which was noted in 90% of nodes assessed here.

Of note, most LNs in this study (78%) had an identifiable remnant available for characterization, while final nodal volumes were not reached until a median of 13–17 months. The fact that so few nodes achieved complete regression indicates that lack of complete regression should not generally be considered an indication for salvage therapy. In addition, CECTN defined nodal morphology exhibited time-dependent trends, where treated LNs generally became less radiographically dense (decreasing median HU) and more heterogeneous (increasing HU standard deviation). In addition, the proportion of soft tissue volume decreased, while the hypodense/lipid, fluid, and enhancement/calcification components increased (Fig. 2b), the latter of which has been observed in other studies [21, 22]. One interpretation of these findings is following radiation, sterilized lymphoid and tumor components are gradually replaced to by acellular scar tissue that facilitates fluid,

hypodense debris, and mineral entrapment. Hamilton et al. noted the appearance of areas of low attenuation (likely corresponding to the hypodense/lipid and fluid area characterized in this study) was correlated with persistent nodal metastasis. However, increase in the hypodense/lipid and fluid components as seen in this study were generally gradual over time (Fig. 2b), while those described by Hamilton et al., were visually identified during early post-treatment and thus were a product of more rapid development [22]. Future studies assessing patients who do not achieve disease control will aim to better understand these features.

Numerous pre-treatment imaging parameters correlated with nodal regression. Initial higher density (higher median HU) and volume were associated with larger final nodal remnants. Traditionally, post-RT nodal size criteria have been used to guide surgical decision-making. Therefore, we investigated nodal regression kinetics using a time-to-event analysis with <1cm short-axis diameter as the cut point of interest. On multivariate analysis, larger (higher volume and short-axis diameter) nodes with a greater hypodense/lipid component and more heterogeneous nodes (greater HU standard deviation) were associated with reaching a <1 cm short-axis diameter. The findings of this study are concordant with those determined by Sanguineti et al. who investigated oropharyngeal carcinoma nodal response patterns during RT and identified initial nodal CT metrics correlated with nodal volumetric behavior, one of the most consistent of which was CT nodal density [21].

While numerous studies have proposed CT-based criteria to help guide post-RT neck evaluation and management [8, 10, 23, 24], refining such criteria is not the intent of this study, as all patients in our cohort achieved disease control with RT-based treatments alone. We believe the value of the current study is to further develop our understanding of nodal regression in HPV-associated OPCs. Importantly this disease represents a unique subset of head and neck cancer with good prognosis and recent trends towards treatment de-intensification [25, 26]. Therefore, developing a high throughput objective nodal imaging characterization methodology coupled with establishing a reference dataset of controlled LNs, may facilitate future investigation allowing for larger comparison studies, particularly in patients with regional persistence/recurrence and less favorable head and neck cancer subsets (e.g. non-HPV associated disease) while integrating additional clinical variables.

In addition to those inherent in a retrospective study design, other limitations deserve mention. While we included only patients with node-positive HPV-associated oropharyngeal carcinoma, our cohort had relatively modest nodal burden in that no patient exhibited N3 disease and only possessed a median of 2 positive nodes. However, the disease characteristics of this cohort are reflective of practice trends at the time of this study, in that patients with advanced nodal disease were often treated with induction systemic therapy. Additional studies investigating the regression patterns of larger LNs following RT, regression patterns during and after induction systemic therapy, and correlation with other imaging modalities (e.g., PET/CT) are worthy future directions. We also appreciate that batched analysis of longitudinal studies with MATLAB may be viewed by some as cumbersome. We are therefore developing a convenient graphical user interface with an easily interpretable output. Future validation studies might also allow reduction in the number of post-treatment scans analyzed. Another potential limitation was our choice to

assess multiple nodes within the same patient separately; as such nodes may share common properties. However, as each node exhibits unique baseline imaging characteristics corresponding to its specific disease burden, an advantage of this methodology is to be able to facilitate future comparisons between non-controlled with controlled nodes when both occur within the same individual.

In conclusion, this descriptive imaging study employing quantitative imaging parameters characterizes the pattern, kinetics, and imaging correlates of radiographic LN regression in a homogeneous subset of HPV-associated oropharyngeal carcinoma radiation responders. These findings support our current nodal imaging response assessment paradigm, propose a simple quantitative methodology, and describe a reference dataset to serve as the basis for further validation and comparison studies. Finally, it is important to note that the objective of this study is to establish proof of concept within a homogenous controlled reference database. We aim to expand this analysis and to investigate regression patterns in patients who do not achieve disease control or later develop disease progression, in other head and neck cancer disease sites, and following induction systemic therapy, while integrating additional clinical variables and imaging modalities (i.e. PET/CT and MRI).

References

1. Chaturvedi AK, Engels EA, Pfeiffer RM, Hernandez BY, Xiao W, Kim E, et al. Human papillomavirus and rising oropharyngeal cancer incidence in the United States. J Clin Oncol. 2011; 29:4294–301. [PubMed: 21969503]
2. Cantrell SC, Peck BW, Li G, Wei Q, Sturgis EM, Ginsberg LE. Differences in imaging characteristics of HPV-positive and HPV-Negative oropharyngeal cancers: a blinded matched-pair analysis. AJNR American journal of neuroradiology. 2013; 34:2005–9. [PubMed: 23660291]
3. Marur S, D'Souza G, Westra WH, Forastiere AA. HPV-associated head and neck cancer: a virus-related cancer epidemic. Lancet Oncol. 2010; 11:781–9. [PubMed: 20451455]
4. Morani AC, Eisbruch A, Carey TE, Hauff SJ, Walline HM, Mukherji SK. Intranodal cystic changes: a potential radiologic signature/biomarker to assess the human papillomavirus status of cases with oropharyngeal malignancies. Journal of computer assisted tomography. 2013; 37:343–5. [PubMed: 23674003]
5. Peters LJ, Weber RS, Morrison WH, Byers RM, Garden AS, Goepfert H. Neck surgery in patients with primary oropharyngeal cancer treated by radiotherapy. Head Neck. 1996; 18:552–9. [PubMed: 8902569]
6. Yom SS, Garden AS, Staerkel GA, Ginsberg LE, Morrison WH, Sturgis EM, et al. Sonographic examination of the neck after definitive radiotherapy for node-positive oropharyngeal cancer. AJNR American journal of neuroradiology. 2011; 32:1532–8. [PubMed: 21757532]
7. Tang C, Komakula S, Chan C, Murphy JD, Jiang W, Kong C, et al. Radiologic assessment of retropharyngeal node involvement in oropharyngeal carcinomas stratified by HPV status. Radiother Oncol. 2013; 109:293–6. [PubMed: 24103114]
8. Liauw SL, Mancuso AA, Amdur RJ, Morris CG, Villaret DB, Werning JW, et al. Postradiotherapy neck dissection for lymph node-positive head and neck cancer: the use of computed tomography to manage the neck. J Clin Oncol. 2006; 24:1421–7. [PubMed: 16549836]
9. Clavel S, Charron MP, Belair M, Delouya G, Fortin B, Despres P, et al. The role of computed tomography in the management of the neck after chemoradiotherapy in patients with head-and-neck cancer. Int J Radiat Oncol Biol Phys. 2012; 82:567–73. [PubMed: 21310545]
10. Hamilton JD, Ahmed S, Sandulache VC, Daram SP, Ow TJ, Skinner HD, et al. Improving Imaging Diagnosis of Persistent Nodal Metastases after Definitive Therapy for Oropharyngeal Carcinoma: Specific Signs for CT and Best Performance of Combined Criteria. AJNR American journal of neuroradiology. 2013

11. Liauw SL, Mancuso AA, Morris CG, Amdur RJ, Mendenhall WM. Definitive radiotherapy for head-and-neck cancer with radiographically positive retropharyngeal nodes: incomplete radiographic response does not necessarily indicate failure. Int J Radiat Oncol Biol Phys. 2006; 66:1017–21. [PubMed: 17145530]
12. Ojiri H, Mancuso AA, Mendenhall WM, Stringer SP. Lymph nodes of patients with regional metastases from head and neck squamous cell carcinoma as a predictor of pathologic outcome: size changes at CT before and after radiation therapy. AJNR American journal of neuroradiology. 2002; 23:1627–31. [PubMed: 12427611]
13. Ahuja A, Ying M. Sonography of neck lymph nodes. Part II: abnormal lymph nodes. Clinical radiology. 2003; 58:359–66. [PubMed: 12727163]
14. Mancuso AA, Maceri D, Rice D, Hanafee W. CT of cervical lymph node cancer. AJR American journal of roentgenology. 1981; 136:381–5. [PubMed: 6781263]
15. van den Brekel MW, Stel HV, Castelijns JA, Nauta JJ, van der Waal I, Valk J, et al. Cervical lymph node metastasis: assessment of radiologic criteria. Radiology. 1990; 177:379–84. [PubMed: 2217772]
16. Mancuso AA, Harnsberger HR, Muraki AS, Stevens MH. Computed tomography of cervical and retropharyngeal lymph nodes: normal anatomy, variants of normal, and applications in staging head and neck cancer. Part II: pathology. Radiology. 1983; 148:715–23. [PubMed: 6878692]
17. Rosenthal DI, Asper JA, Barker JL Jr, Garden AS, Chao KS, Morrison WH, et al. Importance of patient examination to clinical quality assurance in head and neck radiation oncology. Head Neck. 2006; 28:967–73. [PubMed: 16823872]
18. Trojanowska A, Trojanowski P, Bisdas S, Staskiewicz G, Drop A, Klatka J, et al. Squamous cell cancer of hypopharynx and larynx - evaluation of metastatic nodal disease based on computed tomography perfusion studies. European journal of radiology. 2012; 81:1034–9. [PubMed: 21324623]
19. Gregoire V, Levendag P, Ang KK, Bernier J, Braaksma M, Budach V, et al. CT-based delineation of lymph node levels and related CTVs in the node-negative neck: DAHANCA, EORTC, GORTEC, NCIC, RTOG consensus guidelines. Radiother Oncol. 2003; 69:227–36. [PubMed: 14644481]
20. Camp RL, Dolled-Filhart M, Rimm DL. X-tile: a new bio-informatics tool for biomarker assessment and outcome-based cut-point optimization. Clinical cancer research: an official journal of the American Association for Cancer Research. 2004; 10:7252–9. [PubMed: 15534099]
21. Sanguineti G, Ricchetti F, Wu B, Agrawal N, Gourin C, Agbahiwe H, et al. Volumetric change of human papillomavirus-related neck lymph nodes before, during, and shortly after intensity-modulated radiation therapy. Head Neck. 2012; 34:1640–7. [PubMed: 22267196]
22. Hamilton JD, Ahmed S, Sandulache VC, Daram SP, Ow TJ, Skinner HD, et al. Improving imaging diagnosis of persistent nodal metastases after definitive therapy for oropharyngeal carcinoma: specific signs for CT and best performance of combined criteria. AJNR American journal of neuroradiology. 2013; 34:1637–42. [PubMed: 23471023]
23. Ojiri H, Mendenhall WM, Stringer SP, Johnson PL, Mancuso AA. Post-RT CT results as a predictive model for the necessity of planned post-RT neck dissection in patients with cervical metastatic disease from squamous cell carcinoma. Int J Radiat Oncol Biol Phys. 2002; 52:420–8. [PubMed: 11872288]
24. Yeung AR, Liauw SL, Amdur RJ, Mancuso AA, Hinerman RW, Morris CG, et al. Lymph node-positive head and neck cancer treated with definitive radiotherapy: can treatment response determine the extent of neck dissection? Cancer. 2008; 112:1076–82. [PubMed: 18186495]
25. Sturgis EM, Ang KK. The epidemic of HPV-associated oropharyngeal cancer is here: is it time to change our treatment paradigms? Journal of the National Comprehensive Cancer Network: JNCCN. 2011; 9:665–73. [PubMed: 21636538]
26. Tang C, Chan C, Jiang W, Murphy JD, von Eyben R, Colevas AD, et al. Concurrent cetuximab versus platinum-based chemoradiation for the definitive treatment of locoregionally advanced head and neck cancer. Head Neck. 2014

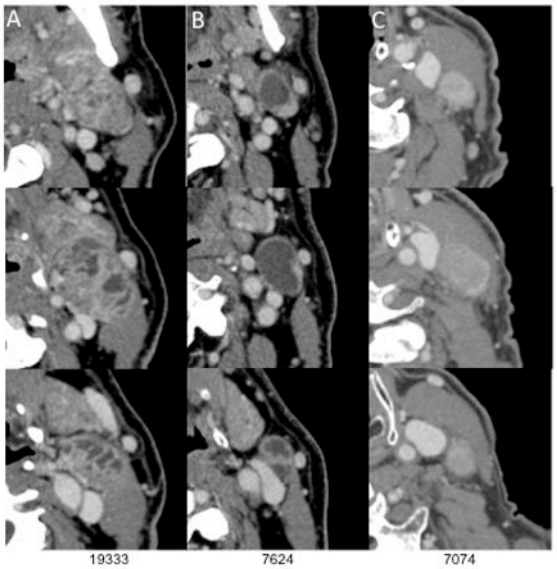

	A	B	C
Volume (mm^3)	19333	7624	7074
Short axis diameter (cm)	2.4	1.7	1.5
Hypodensity/Lipid	0.4%	2.2%	0.1%
Fluid	4.2%	45.4%	0.2%
Soft Tissue	95.3%	52.4%	98.4%
Calcification	0.1%	0%	1.2%
HU median (range)	82 (-68 to 899)	34 (-82 to 147)	124 (-54 to 206)
HU standard Deviation	27	25	22

Figure 1.

Multiple sequential axial pretreatment CT images of representative lymph nodes analyzed: A) complex nodes with numerous smaller cysts; B) predominately cystic node containing predominately one cyst; and C) predominately solid node without a significant cystic component. Nodal characteristics are listed below for each node.

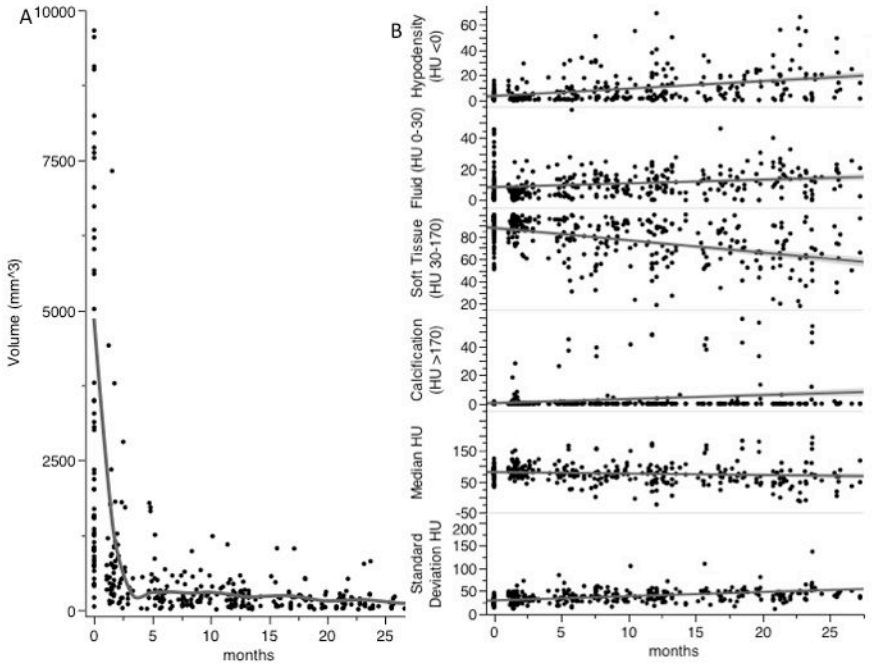

Figure 2.

Lymph node CT characteristics over time from date of radiation therapy completion. A) Node size in mm^3, fitted cubic spline to visualize trend (grey line). B) Node proportion of HU stratified components (% nodal volume-y axis) and node median HU and standard deviation (HU-y axis) over time. Best fit line to visualize trend (grey lines).

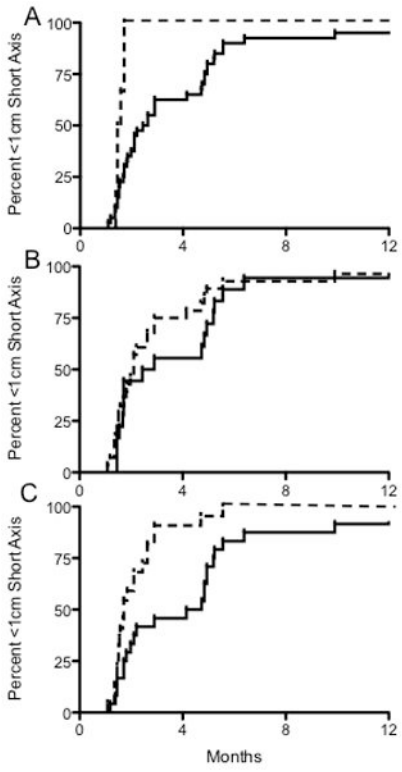

Figure 3.

Cumulative incidence curves showing time to reach <1 cm short axis diameter to illustrate nodal response patterns. A) Stratification by initial percent hypodensity (defined as <0 HU) ≤0.15% (dashed line, n=6) vs. >0.15% (solid line, n=40). B) Stratification by standard deviation ≤23.75 HU (dashed, n=18) vs. > 23.7% HU (solid, n=28). C) Stratification by initial volume ≤5500 mm^3 (dashed, n=22) vs. >5500 mm^3 (solid, n=24).

Table 1

Initial patient and node characteristics

Patient characteristic	Patients (N=36)
Median #Nodes	2 (1–4)
Concurrent systemic therapy	26 (72%)
Males	32 (89%)
Current smokers	6 (17%)
Past smokers	18 (50%)
Median pack years smoking	32 (5–65)
P16 IHC+/HPV ISH+	19 (53%)
P16 IHC+/HPV ISH−	11 (31%)
P16 IHC unknown/HPV ISH+	6 (17%)
T-Stage	
TX	2 (6%)
T1	10 (28%)
T2	15 (42%)
T3	7 (19%)
T4	2 (6%)
N-Stage	
N1	8 (22%)
N2a	3 (8%)
N2b	24 (67%)
N2c	1 (3%)
Primary subsite	
Tonsil	18 (50%)
Base of tongue	18 (50%)

Initial node characteristic	Number lymph nodes (N=66)
HU median	80 (34–124)
HU standard deviation	26 (14–46)
Volume (mm^3)	2311 (60–29565)
Short-axis diameter (mm)	13 (4–32)
% Node	
HU <0 (hypodense)	1 (0–15)
HU 0–30 (fluid)	5 (0–46)
HU 30–170 (soft tissue)	93 (51–100)
HU >170 (enhancing/calcified)	0 (0–2)
Node Site	
Level IB	1 (2%)
Level IIA	51 (77%)
Level IIB	5 (8%)
Level III	7 (8%)
Level IV	2 (3%)

Abbreviations: HU- Hounsfield units

For categorical variables the frequency (percent) is listed. For continuous variables, the median (range) is listed.

Table 2

Univariate and multivariate linear regressions relating initial nodal CT parameters with final volume and short-axis diameter.

Initial node characteristic	Final volume UVA	Final volume MVA	Final short-axis diameter UVA	Final short-axis diameter MVA
% Node HU <0 HU	−7.3 mm^3/%, p=0.23	NI	0.02 mm/% p=0.77	0.23 mm/% p=0.01
% Node HU 0–30 HU	−2.3 mm^3/%, p=0.16	NI	−0.02 mm/% p=0.35	NI
% Node HU 30–170 HU	2.6 mm^3/%, p=0.10	NI	0.01 mm/% p=0.41	NI
% Node HU >170 HU	2.8 mm^3/%, p=0.97	NI	−0.02 mm/% p=0.83	NI
HU median	1.7 mm^3/HU, p=0.08	2.5 cc/HU p=0.004	0.01 mm/HU p=0.16	0.09 mm/HU p=0.008
HU mean	2.1 mm^3/HU, p=0.06	NI	0.02 mm/HU p=0.21	NI
HU standard deviation	−2.6 mm^3/HU, p=0.35	NI	−0.01 mm/HU p=0.66	−0.06 mm/HU p=0.10
Initial volume	0.01 mm^3/cc, p=0.0002	0.01 mm^3/HU p<0.0001	0.0001 mm/cc p=0.007	0.0002 mm/cc p=0.0001
Short axis diameter	9.8 mm^3/mm, p=0.002	NI	0.08 mm/mm p=0.02	NI

Abbreviations: UVA- univariate analysis, MVA- multivariate analysis, HU- Hounsfield units

Slope of the linear regression is displayed for each variable representing unit change in final volume (in cc's) or short-axis diameter (in mm) per unit change in the initial node characteristic listed.

Table 3

Univariate and multivariate time-to-event analysis to <1 cm nodal diameter.

Initial node characteristic	UVA	MVA
% Node HU <0 HU	0.2 (>0.15%)**,&&	0.2, p=0.003
% Node HU 0–30 HU	0.7 (>1.38%)	-
% Node HU 30–170 HU	1.5 (>98%)	-
% Node HU >170 HU	1.2 (>0.15%)	-
HU median	2.1 (>75 HU)*	-
HU mean	1.3 (>70 HU)	-
HU standard deviation	1.3 (>23.75)	1.9, p=0.049
Volume	0.4 (>5500)**	0.4, p=0.020
Short-axis diameter	0.1 (>1.05 cm)**,&&	0.2, p=0.004

Abbreviations: UVA- univariate analysis, MVA- multivariate analysis, HU- Hounsfield units

Hazard ratios (optimal cutpoints) displayed for each pre-treatment parameter for univariate analysis. Hazard ratios and p-values displayed for multivariate analysis.

For univariate analysis:

* p<0.05 and

** p<0.01 unadjusted log-rank p-values.

& p<0.05 and

&& p<0.01 adjusted Miller-Seigmund p-values (adjusting for multiple comparisons)